energies

MDPI

Article

Ag Nanowires/C as a Selective and Efficient Catalyst for CO_2 Electroreduction

Li Zeng, Jun Shi, Hanxin Chen * and Chong Lin *

School of Mechanical and Electrical Engineering, Wuhan Institute of Technology, Wuhan 430205, China; li_zeng@wit.edu.cn (L.Z.); shijunresearch2016@163.com (J.S.)

* Correspondence: pg01074075@163.com (H.C.); chonglin@wit.edu.cn (C.L.); Tel.: +86-139-8602-6473 (H.C.); +86-136-2728-4232 (C.L.)

Abstract: The development of a selective and efficient catalyst for CO_2 electroreduction is a great challenge in CO_2 storage and conversion research. Silver metal is an attractive alternative due to its enhanced catalytic performance of CO_2 electroreduction to CO. Here, we prepared Ag nanowires anchored on carbon support as an excellent electrocatalyst with remarkably high selectivity for the CO_2 reduction to CO. The CO Faradic efficiency was approximately 100%. The enhanced catalytic performances may be ascribed to dense active sites exposed on the Ag nanowires' high specific surface area, by the uniform dispersion of Ag nanowires on the carbon support. Our research demonstrates that Ag nanowires supported on carbon have potential as promising catalysts in CO_2 electroreduction.

Keywords: Ag nanowires; carbon support; electrocatalysis; CO_2 reduction; syngas

Citation: Zeng, L.; Shi, J.; Chen, H.; Lin, C. Ag Nanowires/C as a Selective and Efficient Catalyst for CO_2 Electroreduction. *Energies* **2021**, *14*, 2840. https://doi.org/10.3390/en14102840

Received: 23 March 2021
Accepted: 7 May 2021
Published: 14 May 2021

1. Introduction

With the continuous consumption of fossil fuels, the anthropogenic global warming caused by CO_2 emissions into the atmosphere has attracted significant attention to the energy storage and conversion research field [1–3]. CO_2 conversion to useful fuel/chemical feedstock can alleviate the challenging environmental problems [4–6]. The utilization of renewable energy, for instance, solar and wind, during this conversion is promising. However, the intermittent properties of these resources restrict their further application. By comparison, the defects can be overcome by the electrocatalysis of CO_2 gas into energy fuels [7,8]. Boosting the selectivity and efficiency of CO_2 reduction is the overarching challenge for industrializing CO_2 reduction. Aqueous electrocatalytic reduction of CO_2 at ambient temperature, which is a cost-effective method compared with the electrocatalysis in ionic liquids, has attracted significant attention recently [9,10]. Nevertheless, the electrocatalytic reduction of CO_2 in aqueous solution continually competes with the hydrogen evolution reaction (HER), which is a side reaction accompanying CO_2 reduction [11,12]. Thus, an efficient electrocatalyst with high selectivity is crucial for the fulfillment of energy conversion [13].

Metallic catalysts are appealing for CO_2 electroreduction due to their excellent catalytic activity and selectivity [14–17]. It is acknowledged that CO is an indispensable constituent of syngas (a mixture of CO and H_2), which is generally used to produce Fischer–Tropsch fuels such as gasoline, methanol and ammonia [18,19]. Gold (Au) [20,21], silver (Ag) [22,23], palladium (Pd) [24,25] and zinc (Zn) [26,27], which exhibit outstanding selectivity to CO, have been demonstrated to be efficient electrocatalysts for CO_2 reduction. Nevertheless, gold and palladium are improper for large-scale utilization owing to their rarity and costliness [28]. Zinc possesses poorer stability compared with the other three metals [29]. Silver provides an appreciable compromise between expense and performance and is an attractive option.

Three-dimensional porous Ag, or Ag foam electrodes, present remarkable Faradic efficiencies of CO, over 90% [30,31]. However, a large quantity of Ag is required to achieve high catalytic activity on these macroscopic Ag bulk electrodes, which is the inherent defect of Ag bulk materials. Nanostructured Ag catalysts provide a multitude of active sites for CO_2 reduction owing to their high specific surface areas, thus surpassing bulk materials in efficiency and selectivity [32]. Salehi-Khojin et al. demonstrated that Ag nanoparticles with a size of 5 nm exhibited CO_2 conversion rates 10 times higher than bulk silver [33]. Liu et al. indicated that triangular silver nanoplates possessed a remarkably greater Faradaic efficiency of 96.8%, superior durability of up to 7 days, and an ultralow overpotential of 96 mV, which is attributed to the shape-controlled structure optimizing the edge-to-corner ratio and facets with low activation energy to initiate CO_2 reduction [34]. Luan et al. reported that readily prepared large-scale silver nanowire arrays, with a diameter of 200 nm, exhibited enhanced current density with an efficiency over 90% under a moderate potential of −0.49 V [35]. Liu et al. investigated the catalytic activity of Ag nanowires of 25 nm diameter, achieving a maximum Faradaic efficiency of 99.3%, remarkably low overpotential, and excellent durability [36]. Furthermore, a Ag catalyst alloying with other metals also displayed enhanced catalytic activity [37–39]. Despite the intrinsic performance of Ag nanocatalysts which is evidently reinforced via modification, the shortcoming is that discrete nanostructured catalysts are dispersed on the glass carbon electrode (GCE) inhomogeneously, thus the electrical conductivity is weakened and the catalytic performance is degraded. The application of support can promote electron transfer to the active sites by intense coupling between the catalyst particles and the support, consequently improving the catalytic activity of the nanoparticles [40].

In this study, silver nanowires (Ag NWs) with a diameter of ~200 nm, supported on carbon, were synthesized using the facile polyol-based method. The characterization analysis indicated that Ag NWs were uniformly scattered on the carbon support without accumulation. The as-fabricated Ag NWs/C displayed outstanding catalytic performance in the CO_2 reduction reaction (CO_2RR) with a remarkably enhanced Faradaic efficiency, comparable to that of Ag nanowires with a diameter of 25 nm, as reported by Liu et al., and superior to that of silver nanowire arrays with a similar diameter.

2. Materials and Methods

2.1. Synthesis of Ag NWs/C

In brief, 0.2 g of poly(vinylpyrrolidone) (PVP, 58,000 g mol^{-1}) was first dissolved in 50 mL of ethylene glycol (EG) by continuous agitation at ambient temperature. Then, 0.25 g of silver nitrate ($AgNO_3$) was dissolved in the PVP/EG solution and transparent liquid mixtures were achieved. Next, 19.2 mg of $FeCl_3$ was added to 20 mL of EG. Then, 200 µL of $FeCl_3$ /EG mixtures was transferred into the $AgNO_3$/PVP/EG mixtures and stirred for 2 min to form a uniform solution. Finally, 160 mg amorphous carbon black (CB, CABOT, VXC72) was added into the mixture, which was then decanted to an autoclave for generating Ag NWs/C at 130 °C for 5 h. The as-fabricated precipitation was cleaned with deionized water and ethyl alcohol, followed by centrifugation and freeze-drying treatment. As a reference, powders consisting of 5 mg of Ag bulk and 5 mg of carbon black were mixed.

2.2. Characterization of Ag NWs/C

The chemical phase structure of the as-obtained Ag NWs/C catalyst was determined by powder X-ray diffraction (XRD) with Rigaku Rotaflex Cu Kα radiation. The mass fraction of Ag NWs from Ag NWs/C composites was ascertained by Leeman inductively coupled plasma-atomic emission spectrometry (ICP-AES). The micromorphologies of the catalyst were identified by Zeiss Sigma field emission scanning electron microscopy (FESEM) with an acceleration voltage of 10 kV. Transmission electron microscopy (TEM) and high-resolution transmission electron microscope (HRTEM) were conducted on a JEOL JEM 2100 microscope, which was operated at an accelerating voltage of 200 kV.

2.3. Electrochemical Measurements

All electrochemical measurements of CO_2 reduction were performed in a homemade three-electrode electrochemical H-cell, as shown in Figure 1. The two compartments were segregated by a piece of Nafion 117 membrane. A CHI 660E potentiostat was employed for the electrochemical tests. The catalyst-coated GCE was the working electrode. To fabricate the working electrode, 10 mg of Ag NWs/C was dispersed in the mixed solvent, consisting of 700 μL of isopropanol, 200 μL of deionized water and 100 μL of 5.0 wt.% Nafion solution to form a homogeneous ink by half hour ultrasonic treatment. Afterwards, 5.0 μL of catalyst ink was transferred onto a GCE with a diameter of 5 mm and solid loading of about 0.26 mg cm^{-2}. The GCE was naturally air-dried at ambient temperature. A platinum plate was used as the auxiliary electrode and a saturated calomel electrode as the reference electrode. The electrolyte adopted was 0.1 M $KHCO_3$ solution. The electrochemical tests were carried out atmospherically at room temperature (25 °C). The electrolyte was deaerated via bubbling Ar or CO_2 gas at 20 mL min^{-1} for 2 h before each electrochemical test to assure an Ar or CO_2 saturation state. During the electromechanical measurements, Ar or CO_2 gas was continuously purged into the solution to preserve saturation levels throughout the tests. Linear sweep voltammetries (LSVs) were carried out at a scanning rate of 20 mV s^{-1}. The durability of the catalysts was tested in CO_2-saturated electrolytes with a potentiostatic pattern for 40 h. All the measured potentials were reported with respect to a reversible hydrogen electrode (RHE) by E (V vs. RHE) = E (V vs. SCE) + 0.241 V + 0.0592 × pH with the iR drop calibration by $E_{actual} = E_{measure} - iR_{solution}$.

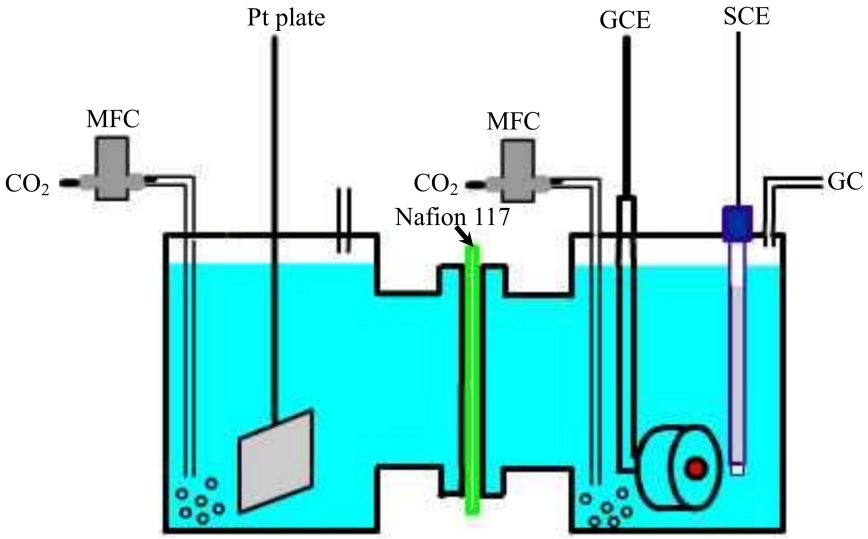

Figure 1. Schematic illustration of three-electrode electrochemical H-cell.

2.4. Product Analysis

To determine the products of CO_2 reduction, and corresponding FEs and selectivity, potentiostatic electrolysis was imposed on the Ag NWs/C and Ag bulk-modified GCE. Briefly, 50 μL of catalyst ink was transferred onto a GCE of 10 mm diameter (solid loading ~0.64 mg cm^{-2}). The gas phase products in the cathode compartment were quantified by Agilent 6890N gas chromatography (GC). The liquid-phase products were analyzed via ^1H nuclear magnetic resonance (NMR). The electrolyte in the cathode compartment was agitated with continuous CO_2 gas purging throughout the electrolysis process. The FEs of gaseous products were determined in S1 in supplementary materials.

3. Results and Discussion

The XRD pattern of Ag NWs/C illustrated in Figure 2 shows that diffraction peaks appearing at 38.6, 44.8, 64.9, 77.8 and 81.8° corresponded to (111), (200), (220), (311) and (222) planes of face-centered cubic Ag (JCPDS No. 87-0719). It is noteworthy that a signal

for the peak of carbon black (002) was not observed, which is ascribed to the faint signals of amorphous carbon black overlaid by the intense diffraction peaks of Ag NWs with excellent crystalline quality [41,42]. The XRD analysis demonstrated that pure Ag NWs supported on carbon were mildly fabricated. The mass fraction of Ag loaded on carbon was 86.9%.

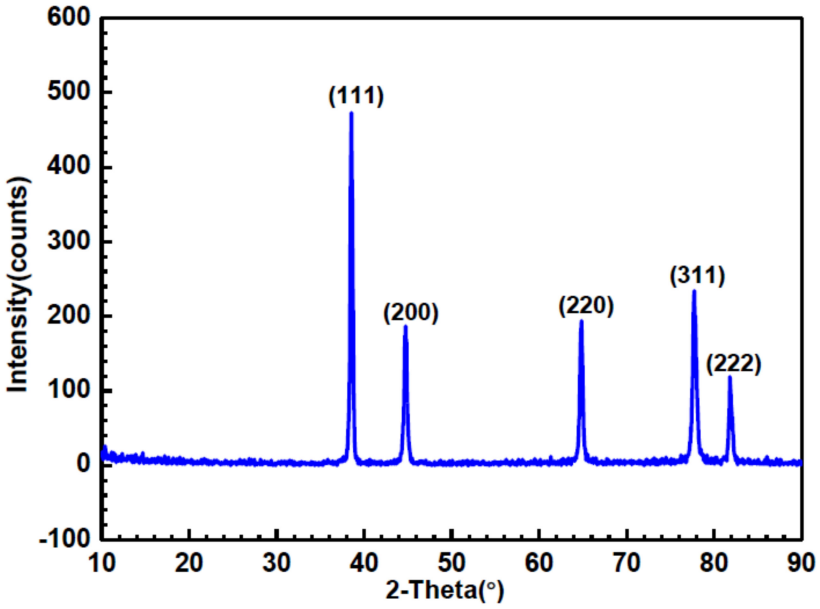

Figure 2. XRD patterns of AgNWs/C.

The micromorphology and microstructure of Ag NWs/C were characterized by SEM and TEM. It can be seen from the SEM image under lower magnification (Figure 3a) that loose Ag NWs were uniformly distributed without accumulation, which is due to excellent dispersion of Ag NWs by the carbon support. The SEM image under higher magnification shows that the prepared Ag NWs possessed a smooth surface with the diameter normally in the range from 200 to 400 nm. The lengths of Ag NWs were up to hundreds of micrometers.

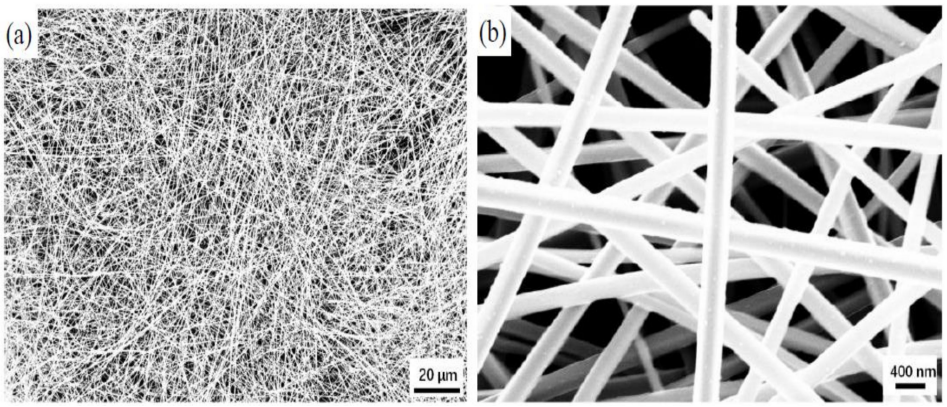

Figure 3. SEM images of (**a**) Ag NWs/C under lower magnification, (**b**) Ag NWs/C under higher magnification.

The carbon support was not obviously observed, which may be a result of the amount of carbon black added in the process of synthesizing the catalyst. By contrast, Ag NWs with 0, 300 mg and 640 mg of carbon black were synthesized as shown in Figure 4. It is observed that the Ag NWs without carbon black are formed with considerable accumulation. Large pieces of silver can also be observed. The Ag NWs were scattered on the flocculent carbon support for Ag NWs with 300 mg of carbon black. However, for Ag NWs with 640 mg of carbon black, the Ag NWs were largely covered by carbon support.

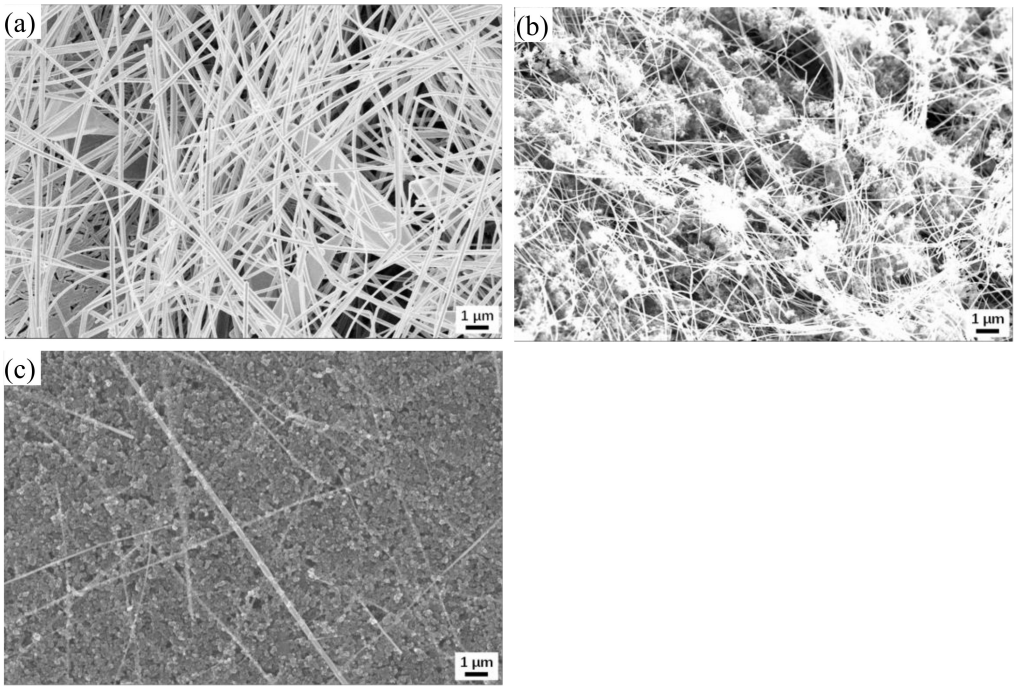

Figure 4. SEM images of (**a**) Ag NWs; (**b**) Ag NWs + 300 mg carbon black; (**c**) Ag NWs + 640 mg carbon black.

The TEM images in Figure 5 show that the Ag NWs were of several micrometers in length with a width of about 200 nm, which is consistent with those observed by SEM. The HRTEM images in the inset further confirmed the successful fabrication of Ag NWs nanocrystallines with interfringe distances of 0.231 nm and 0.207 nm, which correspond to (111) and (200) planes of Ag NWs, respectively. The crystalline structure captured in the HRTEM images was in agreement with the analysis from XRD data.

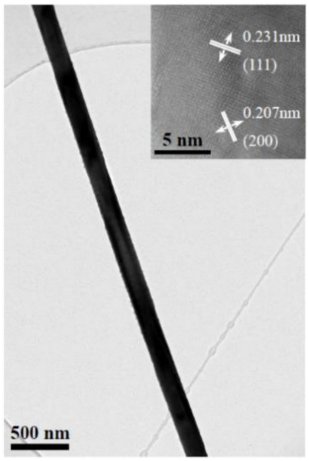

Figure 5. TEM images of Ag NWs/C and corresponding HRTEM images (inset).

The catalytic activity of the as-prepared Ag NWs/C was evaluated by electrochemical measurements. Figure 6a depicts the LSVs of the Ag NWs/C catalyst where the 0.1 M $KHCO_3$ electrolyte was saturated with Ar and CO_2 gas. The onset potential initiating CO_2 reduction was −0.32 V with a maximum current density of 1.46 mA cm^{-2} in CO_2-saturated solution. The onset potential was observed at −0.50 V, and the maximum current density was only 0.55 mA cm^{-2} in Ar-saturated solution. By comparison, the cathodic current density gained in CO_2-saturated solution was much higher (~2.7-fold) and the onset potential was considerably more positive than those under Ar-saturation, which is attributed to reactions of CO_2 reduction in parallel with HER. CVs of Ag NWs/C catalyst,

where the 0.1 M $KHCO_3$ electrolyte was saturated with Ar and CO_2 gas, also showed much higher cathodic current density and more positive onset potential in CO_2-saturated solution. LSVs for Ag NWs/C and Ag bulk in CO_2-saturated solution are shown in Figure 6b. It can be seen that Ag bulk exhibited a reduction current density of 1.49 mA cm^{-2} at −0.83 V, while Ag NWs/C displayed a higher current density of 1.77 mA cm^{-2} at −0.82 V, manifesting enhanced cathodic kinetics of Ag NWs/C catalyst for CO_2 electroreduction, which is also evidenced by comparing CVs for Ag NWs/C and Ag bulk in CO_2-saturated solution. The value of ECSA of the Ag NWs- and Ag bulk-modified electrode was 3.88 cm^2 and 3.75 cm^2 (See Figure S1 in Supplementary Materials). Therefore, the current densities calculated by the electrode geometric area is used in present study.

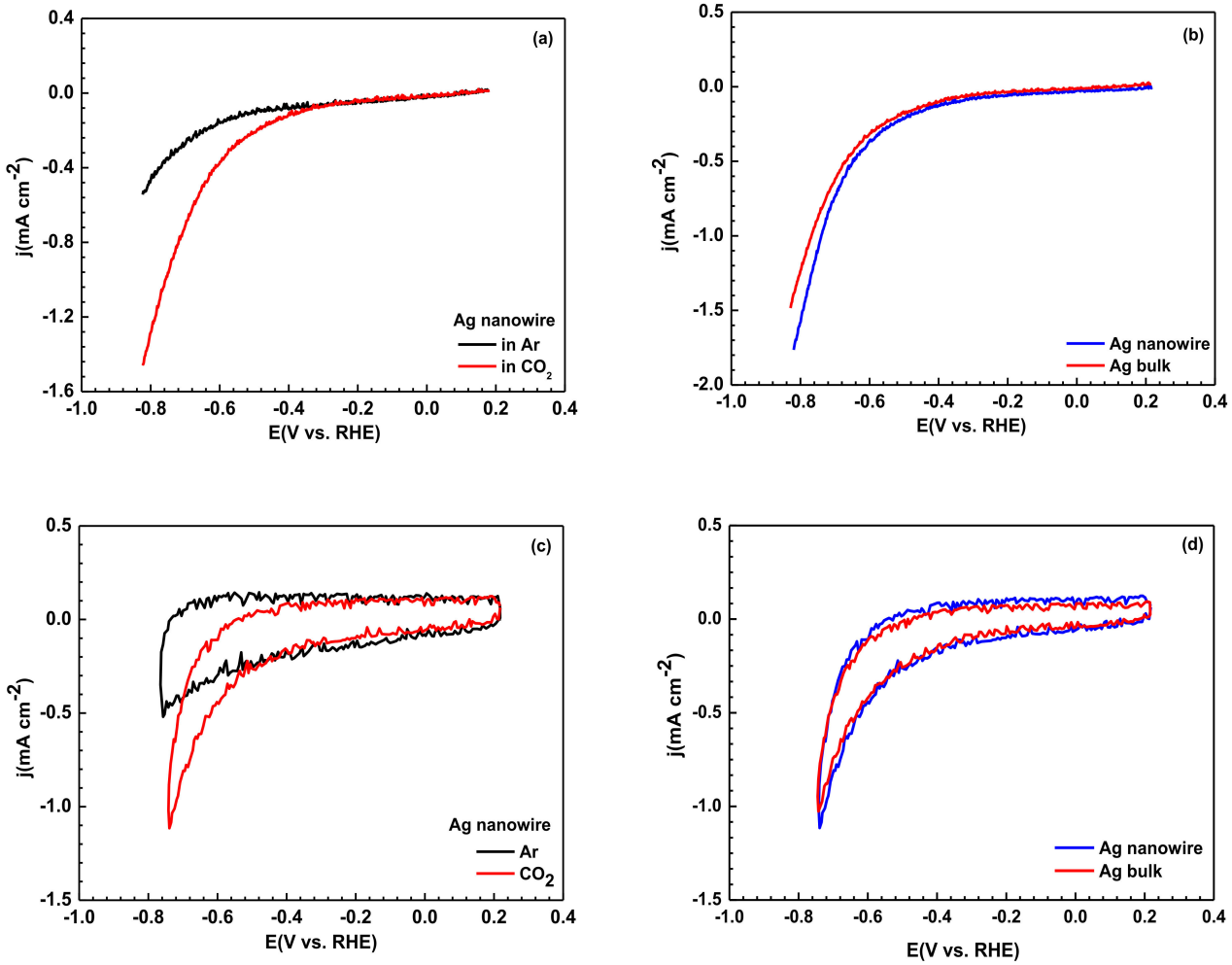

Figure 6. (**a**) LSV for Ag NWs/C in Ar- and CO_2-saturated 0.1 M $KHCO_3$ electrolyte; (**b**) LSV for Ag NWs/C and Ag bulk in CO_2-saturated solution; (**c**) CV for Ag NWs/C in Ar- and CO_2-saturated 0.1 M $KHCO_3$ electrolyte; (**d**) CV for Ag NWs/C and Ag bulk in CO_2-saturated solution.

To verify the occurrence of CO_2RR driven by Ag NWs/C, electrolysis under potentiostatic pattern at different potentials combining with GC and NMR was performed. FEs of gas-phase products over the Ag NWs/C catalyst are shown in Figure 7a. The distributions of gas-phase products demonstrated that CO and H_2 were the major gaseous products (See Tables S1 and S2 in Supplementary Materials), and no liquid products were detected during the electrolysis process. The variation of FEs with the applied potentials demonstrated that the synthesized Ag NWs/C catalyst was highly selective (exceeding 90%) to CO products, ranging from −0.650 V to −0.718 V, with the maximum FE of CO reaching 100% at −0.67 V. The maximum FE of CO was much higher than that (84%) of the Ag nanowire arrays electrode of 200 nm in diameter, as reported by Luan et al. [35] and comparable to that

(99.3%) with five-fold twinned Ag NWs of 25 nm diameter, as reported by Liu et al. [36]. A mixture of CO and H_2, which is known as syngas, was formed with the drop of potential. The FEs of Ag bulk are shown in Figure 7b for comparison. Clearly, Ag NWs/C exhibited significantly higher FEs over the range of the applied potentials. Furthermore, CO gas could only be detected at the potentials more negative than −0.58 V for Ag bulk, with the maximum FE of 41% obtained at the considerably negative potential of −0.86 V. Comparatively, the maximum FE of Ag NWs/C was ~2.4-fold higher than Ag bulk, demonstrating that Ag NWs/C outperform Ag bulk in catalytic selectivity and efficiency. To obtain further insights into the catalytic selectivity of Ag NWs/C, the partial current densities of CO production at different applied cell potentials for Ag NWs/C and Ag bulk are compared in Figure 8. The value of j_{CO} for Ag NWs/C was 0.23 mA cm^{-2}, which was ~4.6-fold higher than that (0.05 mA cm^{-2}) of Ag bulk at the potential where the maximum FE of Ag NWs/C was obtained. The values of j_{CO} were enhanced as the measured potentials scanned cathodically, demonstrating that CO_2 reduction kinetics were augmented with the more negative applied potential exerted on the Ag NWs/C catalyst.

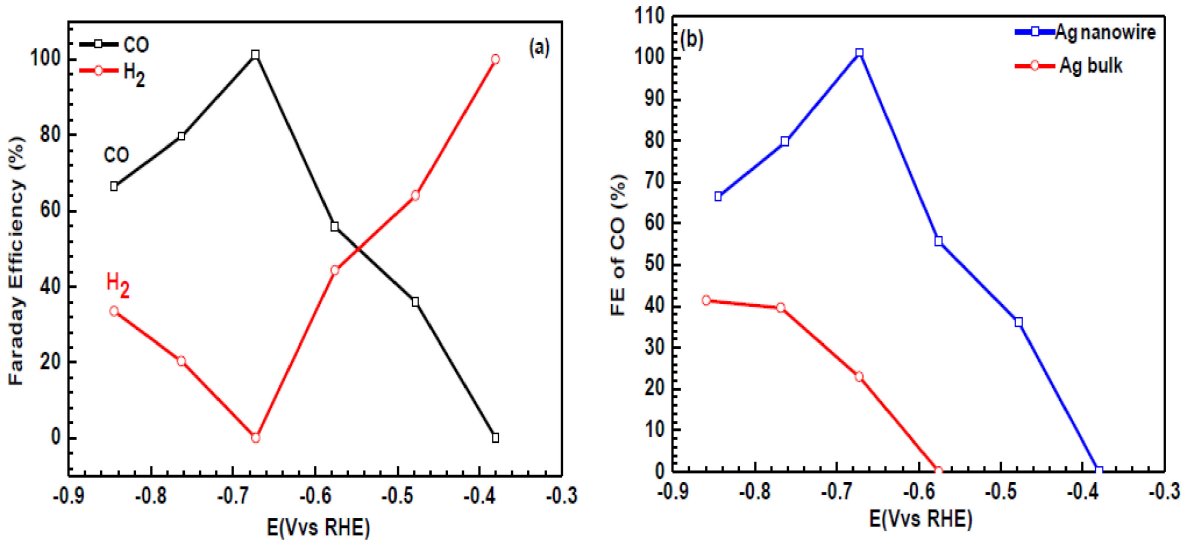

Figure 7. (**a**) FEs of gas-phase products over Ag NWs/C; (**b**) FEs of CO on applied cell potentials for Ag NWs/C and Ag bulk catalysts.

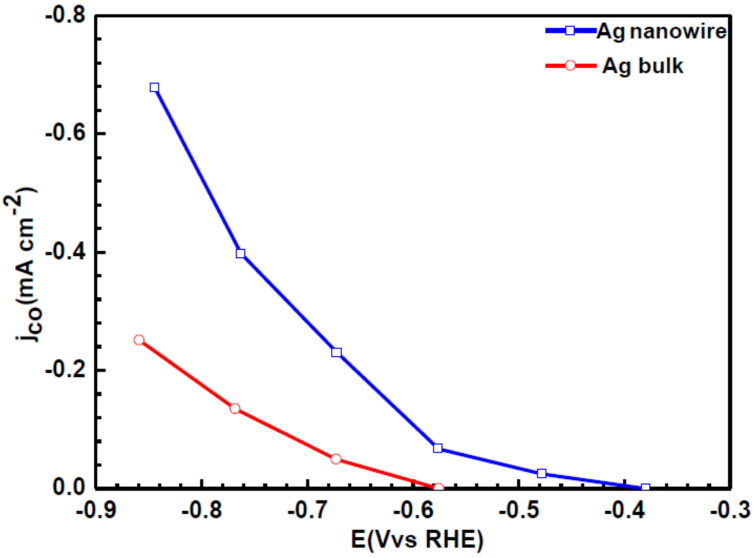

Figure 8. Partial current densities of CO at different applied cell potentials for Ag NWs/C and Ag bulk catalysts.

The Tafel plots of Ag NWs/C and Ag bulk catalysts are plotted in Figure 9 to compare the intrinsic activities. The Tafel slope of 200 mV dec^{-1} for Ag NWs/C was much higher than the theoretical value of 120 mV dec^{-1}, according to the kinetics under the assumption that the first step proceeds at a much more negative potential than the second step in CO_2 electrocatalytic reduction, indicating that the first step is a rate-determining step for CO_2 reduction [23]. Additionally, the Tafel slope achieved from the Ag NWs/C electrode was much lower than that of Ag bulk (260 mV dec^{-1}), suggesting enhanced kinetics with a more prominent intrinsic activity [36]. The durability tests of the prepared Ag NWs/C and Ag bulk catalysts were conducted at the specific potentials of −0.67 V for 40 h, as shown in Figure 10. Remarkably, the current density decayed slowly at the beginning before it became steady, which may be ascribed to the mass-transportation balance process during CO_2 reduction [35]. No apparent slowdown in current density for Ag NWs/C was observed after 40 h testing, while the current density of Ag bulk displayed a continuous decline throughout the testing. CO and H_2 were the gas-phase products, and no liquid products were detected during the potentiostatic measurement at −0.67 V vs. RHE for about 40 h (See Figures S2 and S3 in Supplementary Materials). The FE of CO decreased from 100% to 71.4% during the potentiostatic measurement, indicating that the long-term performance decayed with time.

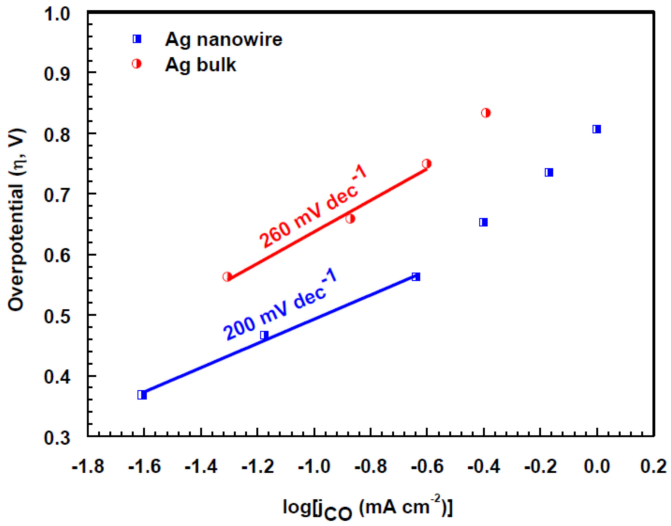

Figure 9. Tafel plots of Ag NWs/C and Ag bulk catalysts.

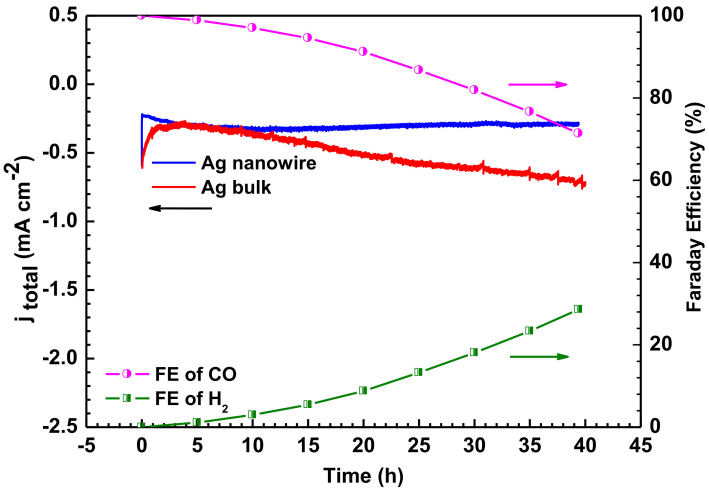

Figure 10. The durability tests of Ag NWs/C and Ag bulk catalysts, and the variation of FE of CO and H_2 with time on Ag NWs/C-modified electrode.

4. Conclusions

Silver nanowires loaded on carbon supports were synthesized for carbon dioxide electroreduction. The Ag NWs/C with a diameter of 200–400 nm exhibited excellent catalytic activity for the CO_2 reduction to CO, with a high CO Faradic efficiency. Our work highlights that Ag NWs with a diameter of hundreds of nanometers, anchored on carbon by facile synthesis, can also provide preeminent catalytic performance.

Supplementary Materials: The following are available online at https://www.mdpi.com/article/10.3390/en14102840/s1, Figure S1: Figure S1. CV curves of (**a**) Ag NWs and (**b**) Ag bulk at different sweep rates; (**c**) The difference between anodic current densities and cathodic current densities at −0.25 V vs. SCE as a function of sweep rates, Figure S2: Spectra of (**a**) FID and (**b**) TCD during potentiostatic measurement at −0.67 V vs RHE, Figure S3. The 1H NMR spectrum for the electrolytic solution prepared with $KHCO_3$ and D_2O after potentiostatic electrolysis at −0.67 V, Table S1: The calibration of GC by standard gas, Table S2: The concentration of CO at different potentials.

Author Contributions: Conceptualization, L.Z.; methodology, J.S.; data curation, C.L.; writing—original draft preparation, L.Z.; writing—review and editing, H.C. All authors have read and agreed to the published version of the manuscript.

Funding: This work was funded by the National Natural Science Foundation of China (Grant No. 51901164), and the National Natural Science Foundation of China (Grant Nos. 51775390, 51805378). This work was also supported by the Science Foundation of Wuhan Institute of Technology (Grant No. K201842).

Institutional Review Board Statement: Not applicable.

Informed Consent Statement: Not applicable.

Data Availability Statement: The data presented in this study are available on request from the corresponding author.

Conflicts of Interest: The authors declare no conflict of interest.

References

1. Rockström, J.; Gaffney, O.; Rogelj, J.; Meinshausen, M.; Nakicenovic, N.; Schellnhuber, H.J. A roadmap for rapid decarbonization. *Science* **2017**, *355*, 1269–1271. [CrossRef]
2. Field, C.B.; Mach, K.J. Rightsizing carbon dioxide removal. *Science* **2017**, *356*, 706–707. [CrossRef]
3. Khezri, B.; Fisher, A.C.; Pumera, M. CO_2 reduction: The quest for electrocatalytic materials. *J. Mater. Chem. A* **2017**, *5*, 8230–8246. [CrossRef]
4. Jones, J.-P.; Prakash, G.K.S.; Olah, G.A. Electrochemical CO_2 reduction: Recent advances and current trends. *Isr. J. Chem.* **2014**, *54*, 1451–1466. [CrossRef]
5. Mistry, H.; Varela, A.S.; Kuhl, S.; Strasser, P.; Cuenya, B.R. Nanostructured electrocatalysts with tunable activity and selectivity. *Nat. Rev. Mater.* **2016**, *1*, 1–14. [CrossRef]
6. Kumar, B.; Llorente, M.; Froehlich, J.; Dang, T.; Sathrum, A.; Kubiak, C.P. Photochemical and photoelectrochemical reduction of CO_2. *Annu. Rev. Phys. Chem.* **2012**, *63*, 541–569. [CrossRef]
7. Gattrell, M.; Gupta, N.; Co, A.C. Electrochemical reduction of CO_2 to hydrocarbons to store renewable electrical energy and upgrade biogas. *Energy Convers. Manage.* **2007**, *48*, 1255–1265. [CrossRef]
8. Whipple, D.T.; Kenis, P.J.A. Prospects of CO_2 utilization via direct heterogeneous electrochemical reduction. *J. Physical. Chem. Lett.* **2010**, *1*, 3451–3458. [CrossRef]
9. Kondratenko, E.V.; Mul, G.; Baltrusaitis, J.; Larrazabal, G.O.; Perezramirez, J. Status and perspectives of CO_2 conversion into fuels and chemicals by catalytic, photocatalytic and electrocatalytic processes. *Energ. Environ. Sci.* **2013**, *6*, 3112–3135. [CrossRef]
10. Mikkelsen, M.; Jørgensen, M.; Krebs, F.C. The teraton challenge. A review of fixation and transformation of carbon dioxide. *Energ. Environ. Sci.* **2010**, *3*, 43–81. [CrossRef]
11. Kuhl, K.P.; Cave, E.R.; Abram, D.N.; Jaramillo, T.F. New insights into the electrochemical reduction of carbon dioxide on metallic copper surfaces. *Energy Environ. Sci.* **2012**, *5*, 7050–7059. [CrossRef]
12. Costentin, C.; Robert, M.; Savéant, J.-M. Catalysis of the electrochemical reduction of carbon dioxide. *Chem. Soc. Rev.* **2013**, *42*, 2423–2436. [CrossRef] [PubMed]
13. Rosen, B.A.; Salehikhojin, A.; Thorson, M.R.; Zhu, W.; Whipple, D.T.; Kenis, P.J.A.; Masel, R.I. Ionic liquid–mediated selective conversion of CO_2 to CO at low overpotentials. *Science* **2011**, *334*, 643–644. [CrossRef]
14. Lu, Q.; Rosen, J.; Jiao, F. Nanostructured metallic electrocatalysts for carbon dioxide reduction. *ChemCatChem* **2015**, *7*, 38–47. [CrossRef]

15. Zhang, S.; Kang, P.; Meyer, T.J. Nanostructured tin catalysts for selective electrochemical reduction of carbon dioxide to formate. *J. Am. Chem. Soc.* **2014**, *136*, 1734–1737. [CrossRef]
16. Qiao, J.L.; Liu, Y.Y.; Hong, F.; Zhang, J.J. A review of catalysts for the electroreduction of carbon dioxide to produce low-carbon fuels. *Chem. Soc. Rev.* **2014**, *43*, 631–675. [CrossRef]
17. Zhu, W.L.; Michalsky, R.; Metin, Ö.; Lv, H.F.; Guo, S.J.; Wright, C.J.; Sun, X.L.; Peterson, A.A.; Sun, S.H. Monodisperse Au nanoparticles for selective electrocatalytic reduction of CO_2 to CO. *J. Am. Chem. Soc.* **2013**, *135*, 16833–16836. [CrossRef]
18. Yang, J.; Ma, W.P.; Chen, D.; Holmen, A.; Davis, B.H. Fischer–Tropsch synthesis: A review of the effect of CO conversion on methane selectivity. *Appl. Catal. A Gen.* **2014**, *470*, 250–260. [CrossRef]
19. Weststrate, C.J.; De Loosdrecht, J.V.; Niemantsverdriet, J.W. Spectroscopic insights into cobalt-catalyzed Fischer-Tropsch synthesis: A review of the carbon monoxide interaction with single crystalline surfaces of cobalt. *J. Catal.* **2016**, *342*, 1–16. [CrossRef]
20. Verma, S.; Hamasaki, Y.; Kim, C.; Huang, W.X.; Lu, S.; Jhong, H.R.M.; Gewirth, A.A.; Fujigaya, T.; Nakashima, N.; Kenis, P.J.A. Insights into the low overpotential electroreduction of CO_2 to CO on a supported gold catalyst in an alkaline flow electrolyzer. *ACS Energy Lett.* **2018**, *3*, 193–198. [CrossRef]
21. Chen, Y.H.; Li, C.W.; Kanan, M.W. Aqueous CO_2 reduction at very low overpotential on oxide-derived Au nanoparticles. *J. Am. Chem. Soc.* **2012**, *134*, 19969–19972. [CrossRef]
22. Dufek, E.J.; Lister, T.E.; Stone, S.G.; Mcilwain, M.E. Operation of a pressurized system for continuous reduction of CO_2. *J. Electrochem. Soc.* **2012**, *159*, F514–F517. [CrossRef]
23. Lu, Q.; Rosen, J.; Zhou, Y.; Hutchings, G.S.; Kimmel, Y.C.; Chen, J.G.; Jiao, F. A selective and efficient electrocatalyst for carbon dioxide reduction. *Nat. Commun.* **2014**, *5*, 3242. [CrossRef] [PubMed]
24. Gao, D.F.; Zhou, H.; Wang, J.; Miao, S.; Yang, F.; Wang, G.X.; Wang, J.G.; Bao, X.H. Size-dependent electrocatalytic reduction of CO_2 over pd nanoparticles. *J. Am. Chem. Soc.* **2015**, *137*, 4288–4291. [CrossRef] [PubMed]
25. Lu, H.; Zhang, L.; Zhong, J.H.; Yang, H.G. Partially oxidized palladium nanodots for enhanced electrocatalytic carbon dioxide reduction. *Chem. Asian J.* **2018**, *13*, 2800–2804. [CrossRef]
26. Nguyen, D.L.T.; Jee, M.S.; Won, D.H.; Jung, H.; Oh, H.-S.; Min, B.K.; Hwang, Y.J. Selective CO_2 reduction on zinc electrocatalyst: The effect of zinc oxidation state induced by pretreatment environment. *ACS Sustain. Chem. Eng.* **2017**, *5*, 11377–11386. [CrossRef]
27. Jiang, X.L.; Cai, F.; Gao, D.F.; Dong, J.H.; Miao, S.; Wang, G.X.; Bao, X.H. Electrocatalytic reduction of carbon dioxide over reduced nanoporous zinc oxide. *Electrochem.Commun.* **2016**, *68*, 67–70. [CrossRef]
28. Ge, J.Y.; Long, J.; Sun, Z.X.; Feng, H.; Hu, J.; Koh, S.W.; Yu, Q.; Xiao, J.P.; Li, H. Vertical silver@silver chloride core–shell nanowire array for carbon dioxide electroreduction. *ACS Appl. Energy Mater.* **2019**, *2*, 6163–6169. [CrossRef]
29. Hu, L.; Zhang, Y.C.; Han, W.Q. Boosting CO_2 electroreduction over silver nanowires modified by wet-chemical sulfidation and subsequent electrochemical de-sulfidation. *New J. Chem.* **2019**, *43*, 3269–3272. [CrossRef]
30. Abeyweera, S.C.; Yu, J.; Perdew, J.P.; Yan, Q.M.; Sun, Y.G. Hierarchically 3D porous Ag nanostructures derived from silver benzenethiolate nanoboxes: Enabling CO_2 reduction with a near-unity selectivity and mass-specific current density over 500 A/g. *Nano Lett.* **2020**, *20*, 2806–2811. [CrossRef]
31. Daiyan, R.; Lu, X.; Ng, Y.H.; Amal, R. Highly selective conversion of CO_2 to CO achieved by a three-dimensional porous silver electrocatalyst. *Chemistryselect* **2017**, *2*, 879–884. [CrossRef]
32. Xi, W.; Ma, R.Z.; Wang, H.; Gao, Z.; Zhang, W.Q.; Zhao, Y.F. Ultrathin Ag nanowires electrode for electrochemical syngas production from carbon dioxide. *ACS Sustain. Chem. Eng.* **2018**, *6*, 7687–7694. [CrossRef]
33. Salehi-Khojin, A.; Jhong, H.-R.M.; Rosen, B.A.; Zhu, W.; Ma, S.C.; Kenis, P.J.A.; Masel, R.I. Nanoparticle silver catalysts that show enhanced activity for carbon dioxide electrolysis. *J. Phys. Chem. C* **2013**, *117*, 1627–1632. [CrossRef]
34. Liu, S.; Tao, H.; Zeng, L.; Liu, Q.; Xu, Z.; Liu, Q.; Luo, J.L. Shape-dependent electrocatalytic reduction of CO_2 to CO on triangular silver nanoplates. *J. Am. Chem. Soc.* **2017**, *139*, 2160–2163. [CrossRef] [PubMed]
35. Luan, C.H.; Shao, Y.; Lu, Q.; Gao, S.H.; Huang, K.; Wu, H.; Yao, K.F. High-performance carbon dioxide electrocatalytic reduction by easily fabricated large-scale silver nanowire arrays. *ACS Appl. Mater. Inter.* **2018**, *10*, 17950–17956. [CrossRef]
36. Liu, S.B.; Wang, X.Z.; Tao, H.B.; Li, T.F.; Liu, Q.; Xu, Z.H.; Fu, X.Z.; Luo, J.L. Ultrathin 5-fold twinned sub-25 nm silver nanowires enable highly selective electroreduction of CO_2 to CO. *Nano Energy* **2018**, *45*, 456–462. [CrossRef]
37. Larrazabal, G.O.; Martin, A.J.; Mitchell, S.; Hauert, R.; Perezramirez, J. Synergistic effects in silver-indium electrocatalysts for carbon dioxide reduction. *J. Catal.* **2016**, *343*, 266–277. [CrossRef]
38. Luc, W.; Collins, C.V.; Wang, S.W.; Xin, H.L.; He, K.; Kang, Y.J.; Jiao, F. Ag–Sn bimetallic catalyst with a core–shell structure for CO_2 reduction. *J. Am. Chem. Soc.* **2017**, *139*, 1885–1893. [CrossRef]
39. Singh, S.N.; Gautam, R.K.; Malik, K.; Verma, A. Ag-Co bimetallic catalyst for electrochemical reduction of CO_2 to value added products. *J. CO2 Util.* **2017**, *18*, 139–146. [CrossRef]
40. Voiry, D.; Fullon, R.; Yang, J.; Silva, C.D.; Kappera, R.; Bozkurt, I.; Kaplan, D.; Lagos, M.J.; Batson, P.E.; Gupta, G. The role of electronic coupling between substrate and 2D MoS_2 nanosheets in electrocatalytic production of hydrogen. *Nat. Mater.* **2016**, *15*, 1003–1009. [CrossRef]
41. Zeng, L.; Shi, J.; Luo, J.L.; Chen, H.X. Silver sulfide anchored on reduced graphene oxide as a high-performance catalyst for CO_2 electroreduction. *J. Power Sources* **2018**, *398*, 83–90. [CrossRef]
42. Zhu, Y.W.; Murali, S.; Cai, W.W.; Li, X.S.; Suk, J.W.; Potts, J.R.; Ruoff, R.S. Graphene and graphene oxide: Synthesis, properties, and applications. *Adv. Mater.* **2010**, *22*, 3906–3924. [CrossRef] [PubMed]